Structure and properties of amorphous hydrogenated silicon carbide

Mark A. Petrich,* Karen K. Gleason,† and Jeffrey A. Reimer
Department of Chemical Engineering, University of California, Berkeley, California 94720-9989
(Received 18 June 1987)

We have studied a compositionally varying series of amorphous hydrogenated silicon carbide (*a*-SiC:H) thin films deposited from silane-methane-hydrogen plasmas. The carbon-bonding enviroments were examined by ^{13}C nuclear magnetic resonance (NMR) while the hydrogen microstructure was characterized by multiple-quantum nuclear magnetic resonance as well as conventional single-quantum solid-state NMR techniques. In addition, Fourier-transform infrared absorption, electron-spin resonance, Rutherford backscattering, and optical-absorption spectra were obtained. The ^{13}C nuclear magnetic resonance spectra showed that all films contain both sp^3 (tetrahedral) and sp^2 (planar) carbon-bonding environments. The sp^3 carbon is predominantly hydrogenated while the sp^2 carbon has no bound hydrogen. Two distinct types of microstructure were found within the compositional series. At low carbon contents (<20 at. %), this alloy system forms "amorphous-silicon-like" lattices, containing clusters of 6 ± 1 hydrogen atoms and regions devoid of hydrogen, due to inclusions of nonhydrogenated sp^2 carbon. Higher-carbon-content samples also consisted of hydrogenated and nonhydrogenated regions, but did not have the well-defined hydrogen microstructure of the lower-carbon-content films. Also, there is a greater fraction of sp^3 carbon in the higher-carbon-content films. The transition between the two types of hydrogen microstructure was clearly reflected in the deposition rates, defect density, disorder, and optical band gaps of the alloy. Thus, the heterogeneous nature of the carbon-atom-bonding configurations and hydrogen microstructure affect the optoelectronic properties of *a*-SiC:H.

I. INTRODUCTION

Amorphous hydrogenated silicon carbide (*a*-SiC:H) has been proposed as a wide-band-gap intrinsic layer in multilayer amorphous silicon (*a*-Si:H) solar cells,[1] and has already been used as a *p*-type window layer in *a*-Si:H solar cells.[2] Stoichiometry affects the optoelectronic properties of amorphous hydrogenated silicon carbide (*a*-SiC:H), creating the possibility of tailoring these alloys for specific applications. However, the behavior of *a*-SiC:H alloys is complicated and many of their properties do not vary linearly with alloy composition.[3] Electron-spin resonance[4] and conductivity measurements[5] show an increase in defect density and disorder with increasing carbon incorporation, limiting the utility of these materials. Many researchers have sought to improve the electro-optical properties of *a*-SiC:H,[5] motivating many structural studies.[6,7] However, several structural issues remain unresolved. Do carbon-carbon bonds exist in *a*-SiC:H with carbon-to-silicon ratios less than 1? Are the carbon atoms in tetrahedral (sp^3) or planar (sp^2) environments? What is the nature of the hydrogen microstructure? The answers to these questions should provide an improved understanding of the relationships among structure, deposition chemistry, and optoelectronic properties of *a*-SiC:H.

Solid-state nuclear magnetic resonance (NMR) is a powerful tool for studying microstructure in amorphous semiconductors. Most researchers using NMR have focused on hydrogen microstructures,[8] although ^{29}Si and ^{13}C have been studied in amorphous silicon[8] and amorphous carbon.[9] This paper reports an investigation of the effects of hydrogen microstructure and carbon local bonding environments on the optoelectronic properties of *a*-SiC:H. The direct structural changes brought about by the incorporation of carbon atoms are accompanied by changes in the hydrogen microstructure. Since hydrogen microstructure is intimately connected with the properties of *a*-Si:H,[10] it should also affect the properties of *a*-SiC:H. We have used multiple-quantum NMR and single-quantum NMR to study the hydrogen microstructure, and magic-angle spinning with dipolar decoupling to study the carbon-local-bonding configurations in *a*-SiC:H. The data reported here show that in materials produced at these conditions carbon-carbon bonding does occur for C/Si ratios less than 1. The data also show that a large fraction of the carbon is bound in sp^2 environments which do not contain hydrogen. The hydrogen microstructures exhibit two behaviors: well-ordered "amorphous-silicon-like" clusters in low-carbon-content films, and large, ill-defined structures in higher-carbon-content films. Additional evidence for this behavior was provided by Fourier-transform infrared absorption, electron-spin resonance (ESR), Rutherford backscattering, and optical-absorption spectra.

II. EXPERIMENT

Samples of *a*-SiC:H were prepared in a plasma-enhanced chemical-vapor-deposition reactor from a mixture of silane (SiH_4), methane (CH_4), and hydrogen (H_2). Prior to each deposition, the reactor was evacuated to 5×10^{-5} torr. The total gas flow rate (49 cm^3/min), pressure (300 mtorr), substrate temperature (270 °C), and

the power density (0.4 W/cm^2) were held constant. These parameters were selected by empirically maximizing the a-Si:H growth rate while minimizing the ESR spin density. The reactant flow rate was 40 cm^3/min (SiH_4+CH_4) diluted with 9 cm^3/min H_2. All flow rates are referenced to "standard conditions" of 760 torr and 0 °C. Samples of different composition were obtained by changing the CH_4-(CH_4+SiH_4) ratio between 0.00 and 0.975. Films were simultaneously deposited onto crystalline silicon, quartz, and aluminum foil. The films were approximately 3 μm thick, as measured by a mechanical stylus. Films deposited on crystalline silicon substrates were used for the ir measurements and those on quartz were used for the optical-absorption measurements. Aluminum foil substrates were removed by a dilute hydrochloric acid etch, yielding approximately 30 mg of material for the proton NMR and ESR measurements. Other samples, approximately 25 μm thick, were deposited on quartz and aluminum foil. The films on quartz were used to determine the Urbach edge, while those on the aluminum were removed and studied with ^{13}C NMR. Samples approximately 500 Å thick were deposited onto beryllium substrates for Rutherford backscattering analysis of the carbon-to-silicon ratios.

Proton NMR data were obtained at 6.3 T (proton frequency equal to 267 MHz) with a homebuilt spectrometer. Absorption spectra were measured by Fourier transforming 20–50 signal-averaged free-induction decays. Integration of the spectra yielded hydrogen contents, with a known weight of hexamethyl benzene serving as a reference. The a-SiC:H NMR line shapes are the sum of a broad Gaussian curve and a narrow Lorentzian curve, indicative of hydrogen in clustered and isolated environments, respectively.[11] Proton spin-lattice relaxation times (T_1) were determined by the inversion recovery method.[12]

The distribution of hydrogen atoms in the samples was studied with multiple-quantum NMR.[13] The details of the experiment have been reported previously in a study of hydrogen microstructure in a-Si:H.[14] The experiment consisted of three periods: preparation, mixing, and detection. During the preparation period, an 8-pulse, 60-μs cycle was repeated an integral number of times. The average Hamiltonian developed by this cycle created even-order multiple-quantum (MQ) coherences, which had changes in the magnetic quantum number of $0, \pm 2, \pm 4, \ldots, \pm 2n$. The mixing period was similar to the preparation period except that each pulse was shifted 90° in phase, creating an average Hamiltonian opposite in sign to that of the preparation period. The mixing period created observable magnetization from the otherwise unobservable MQ coherences. After a 1-ms delay, a $\pi/2$ pulse was used to detect the signal. The entire sequence was repeated for 32 incrementally different phases of the preparation period pulses, accumulating between 5 and 20 signal averages at each phase setting. An interferogram of signal intensities with respect to the phase of the preparation period pulses was Fourier transformed to yield stick spectra of ± 16 MQ coherences. Noise in these spectra appears as odd-order coherences. To simplify the appearance of these spectra, only even-order coherences will be shown. Only positive MQ orders will be shown since the spectra are symmetric.

A series of MQ spectra at different preparation times (60–600 μs) probes the extent of hydrogen clustering. The preparation time required to correlate the behavior of a set of nuclear spins is proportional to the inverse of the dipolar coupling constants among those spins. Because these dipolar coupling constants are inversely proportional to the cube of the distance between the nuclei, different distances are probed by varying the preparation time, yielding information on the spatial distribution of nuclei. For example, if the nuclei are distributed continuously, the intensities of the MQ coherences will grow steadily as the preparation time is increased. If the nuclei exist in isolated clusters, the MQ intensities will plateau at long preparation times. Combinatorial arguments predict that the intensity of the nth-order coherence, $I(n)$, in an isolated cluster of N spins can be described by the Gaussian distribution,

$$I(n)=M\exp(-n^2/N)\ , \tag{1}$$

where M is the magnitude. If there is coupling between clustered environments of equal size, the intensity of the nth-order coherence can be described as the sum of two Gaussian curves,

$$I(n)=M_c\exp(-n^2/N_c)+M_i\exp(-n^2/N_i)\ , \tag{2}$$

where M_c and M_i are the magnitudes, N_c is the number of spins in a cluster, and N_i is indicative of the intercluster interactions.[10,13,14]

The ^{13}C NMR results were obtained at 4.3 T using a homebuilt spectrometer (proton frequency, 180 MHz; ^{13}C frequency, 45 MHz), with a Doty Scientific magic-angle spinning, double-resonance probe. All spectra were taken with a 4000 rotations per second magic-angle spinning rate. Sample sizes for these experiments were between 200 and 350 mg. We observed the ^{13}C free-induction decay after a 90° pulse both with and without proton decoupling during data acquisition. The Fourier-transformed spectra for the lowest-carbon-content sample (13 at. % carbon) are the result of 7500 signal averages, while those for the other samples are the result of 2500 signal averages. In all cases, the delay between averages was 5 sec, which was approximately three times the ^{13}C spin-lattice relaxation time constant. These spectra, shown in Fig. 5, are plotted relative to tetramethylsilane (TMS) on the δ scale (chemical shift of TMS is 0 ppm, benzene + 128.7 ppm, downfield is to the left).

The basic ^{13}C NMR spectrum contains information about many phenomena such as dipole-dipole coupling and chemical-shift anisotropies. Often, the NMR spectra are difficult to interpret because more than one phenomenon is significant. The advantage of using NMR to study local bonding configurations arises from our ability to selectively suppress or enhance the effects of these phenomena. In this study we used two of these selective techniques: proton decoupling and magic-angle spinning. Proton decoupling removes the effect of the ^{13}C-^{1}H dipolar interaction from the spectra.[15] We ob-

serve more features when we use proton decoupling because removing the ^{13}C-^{1}H dipolar coupling leads to longer ^{13}C relaxation times and narrower lines in the Fourier-transformed spectra. By taking spectra with and without proton decoupling, we can study hydrogenated and nonhydrogenated carbon environments. Without proton decoupling, hydrogenated carbon atoms usually relax so rapidly that their Fourier-transformed spectra are too broad to be distinguished from the base line. Magic-angle spinning[16] removes line broadening caused by chemical-shift anisotropies, making it easier to determine which chemical species are present.

Infrared-absorption (ir) spectra were measured with a Digilab Qualimatic FTS-50 Fourier-transform ir spectrometer. A trigallium sulfide detector provided a flat response from 4000 to 400 cm^{-1}. The spectra were the result of 64 signal-averaged scans, Fourier transformed and plotted as absorption spectra. In some regions, overlapping Gaussian absorption curves were resolved by a numerical curve-fitting procedure.

ESR spin densities were measured by comparing the signal intensities from these samples with the intensity from a known sample. The spectrometer (IBM Instruments ER200D-SRC) was sufficiently sensitive to observe these spectra in a single sweep at a center field of 3350 G.

Values of the optical band gap and widths of the Urbach tails were calculated from the optical-absorption spectra from 3000 to 15 000 Å measured with a Cary 14 spectrophotometer. To observe optical-absorption coefficients from 10^2 to 5×10^4 cm^{-1}, two sample thicknesses (4 and 25 μm) were analyzed. The optical band gap was determined by a best fit to Tauc's law[17] in the absorption range 8×10^3 to 5×10^4 cm^{-1}, while the Urbach edge[18] is defined by the reciprocal of the slope of a semilogarithmic plot in the absorption range 9×10^2 to 3×10^3 cm^{-1}.

III. RESULTS

Figure 1 shows the effects of r, the reactant ratio CH_4-(CH_4+SiH_4), on film composition and growth rate. A small amount of methane increases the growth rate slightly over that of a-Si:H. However, for r greater than 0.5, the growth rate decreases sharply. As r increases, the film composition varies nonlinearly. As observed in other work,[3] the carbon-to-silicon ratios in the films are low compared to the ratio of methane-to-silane in the reactant gas mixture. The highest-carbon-content film has a carbon-to-silicon ratio of 1.0 and was prepared from a mixture having a methane-to-silane ratio of 39.0. The hydrogen content of the two lowest-carbon-content samples is lower than the hydrogen content of a-Si:H prepared under the same conditions.

Figure 2 shows how the results of proton NMR measurements change with the addition of methane to the reactant gas mixture. At first ($r=0.25$, 0.50), the spin-lattice relaxation time constant, T_1 [Fig. 2(a)], decreases slightly compared to a-Si:H. A large increase in T_1 occurs at $r=0.795$, followed by a decrease with further carbon incorporation. The overall variation in T_1 (2–4 s) is small compared to the variation seen in a-Si:H samples prepared at different substrate temperatures (2–15 s).[14] The narrow component fraction of the NMR line shape [Fig. 2(b)] decreases monotonically with the CH_4-(CH_4+SiH_4) ratio, in agreement with previous results.[19] The widths of both the narrow Lorentzian and broad Gaussian line shapes [Fig. 2(c)] for the first two carbon alloys ($r=0.25$ and $r=0.50$) are similar to the widths of the Lorentzian and Gaussian components of the a-Si:H spectrum. At higher carbon contents, the widths of both the Lorentzian and Gaussian components increase, with the width of the Gaussian component increasing more. Fitting the sum of two Gaussian curves[19] to the spectra resulted in a larger rms error than fitting the sum of a Gaussian and a Lorentzian curve.

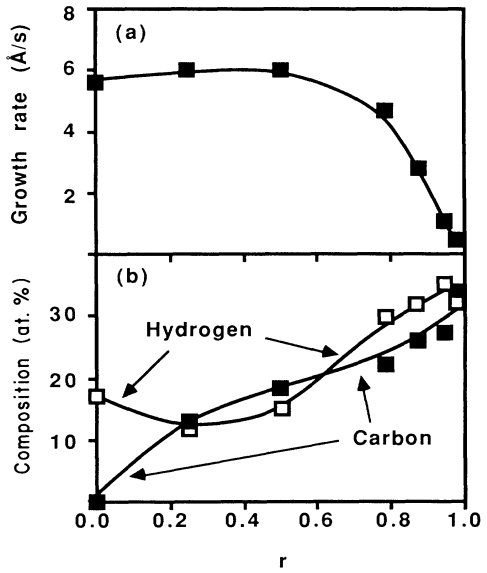

FIG. 1. Film growth rates (a) and composition (b) vs methane fraction in the reactant gases, $r=[CH_4]/[(CH_4+SiH_4)]$. Both the growth rate and carbon content change more rapidly at $r>0.50$. For these measurements, the experimental errors are on the order of the plot symbol size.

The MQ NMR spectra for five of the samples at a preparation time of 180 μs is shown in Fig. 3. The top spectrum is for a-Si:H ($r=0.00$) and the intensities of the second-, fourth-, and sixth-order MQ coherences are greater than the noise. The same coherences are present in the next spectrum ($r=0.25$), although the intensities of the fourth- and sixth-order MQ coherences are slightly larger than in the top spectrum. The intensities of the coherences continue to grow as the CH_4-(CH_4+SiH_4) ratio is increased until, in the bottom spectrum ($r=0.875$), the eighth- and tenth-order MQ coherences are larger than the noise. The largest change in the series occurs between the second ($r=0.25$) and third ($r=0.50$) samples.

To determine the number of correlated nuclear spins, N, as a function of preparation time, each of the multiple-quantum spectra shown in Fig. 3, as well as those taken at other preparation times, are fit with Eq.

(1). This single Gaussian distribution describes the envelope of MQ intensities in the spectra within experimental accuracy for all but the a-Si:H ($r=0.00$) and the first a-SiC:H ($r=0.25$) samples. For these two samples, Eq. (2), the sum of two Gaussian distributions, best describes the data and yields values of the cluster size, N_c. Figure 4 shows the results of these fits for the first four samples of the series. For the a-Si:H sample [Fig. 4(a)], N increases slowly and N_c is constant (6 ± 1 spins) with preparation time. The behavior of the first a-SiC:H [Fig. 4(b)] sample is similar, also having a constant N_c value of 6 ± 1 spins. However, N increases more rapidly with preparation time than for a-Si:H. Although the hydrogen content of the first a-SiC:H sample is 4 at. % less than the a-Si:H sample, the extent of clustering as measured by the magnitude of N, has increased. The next a-SiC:H sample [Fig. 4(c)] shows a steep increase in N even though its hydrogen content is only 1 at. % greater than the first a-SiC:H sample and is still less than that of the a-Si:H sample. The third a-SiC:H sample [Fig. 4(d)], shows the sharpest increase in N with increasing preparation time. The remaining samples, deposited with $r=0.875$, 0.95, and 0.975, show the same MQ behavior as the third a-SiC:H sample.

Figure 5 shows a proton-decoupled magic-angle spinning ^{13}C NMR spectrum of the $r=0.25$ sample (top left), and a spectrum of the same sample without proton decoupling (to right). In the top left spectrum, absorption regions at 120 and 0 ppm correspond to sp^2 carbon (unsaturated, or olefinic) and sp^3 carbon (saturated, or paraffinic), respectively.[20] The spectrum also shows small spinning side bands, which appear at integral multiples of the rotor frequency.[16] The peak widths derive from the number of chemically distinct environments involved. For example, the sp^3 peak can include $-CH_3$, $-C_2H_5$, and other paraffinic groups. It also contains the resonance from C—Si bonds.[21] Carbons forming the sp^2 peak may be doubly bound to other carbon or silicon atoms, and may or may not be hydrogenated. Additionally, in amorphous materials, bond-length and bond-angle distortions broaden the spectrum. Dipolar coupling between ^{13}C atoms could broaden the spectrum, but the low natural abundance (1.11%) of ^{13}C eliminates this broadening. The top right spectrum, without proton decoupling, is very different from the top left spec-

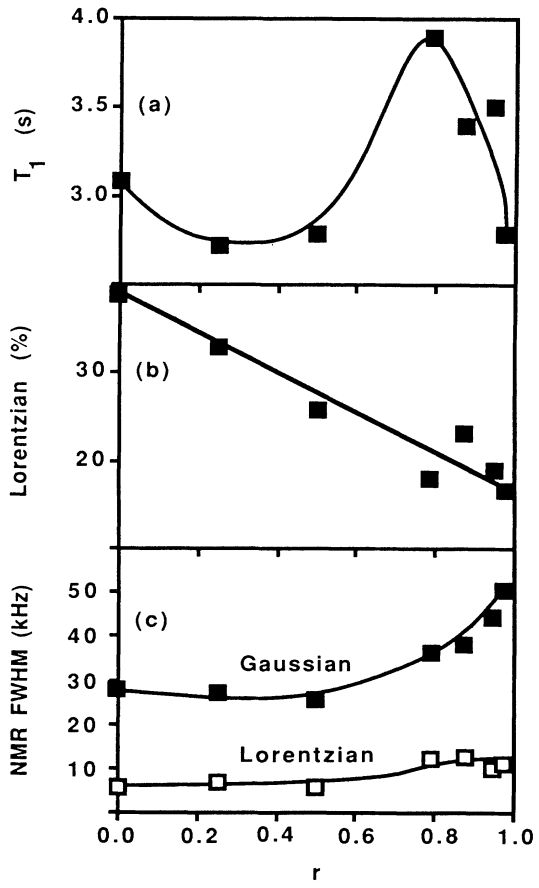

FIG. 2. Single quantum NMR measurements vs $r=[CH_4]/[(CH_4+SiH_4)]$; spin-lattice relaxation time constant (a), percentage of Lorentzian component in the NMR spectrum (b), and the full widths at half maximum (FWHM) of the Lorentzian and Gaussian components (c). The experimental uncertainties are ±0.1 s for (a), $\pm3\%$ for (b), and ±3 kHz for the Gaussian width and ±1 kHz for the Lorentzian width in (c).

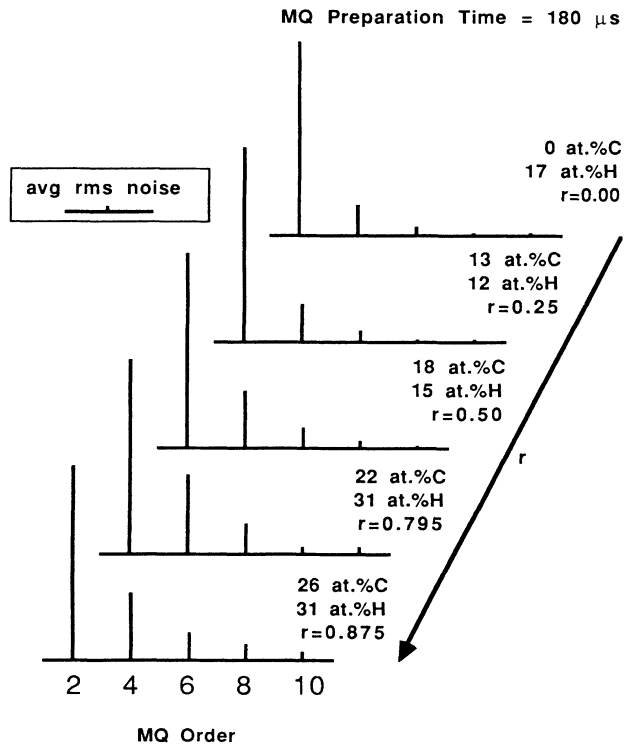

FIG. 3. MQ NMR spectra taken at a preparation time of 180 μs. The number of even-order coherences and their intensities increase with increasing carbon incorporation. The rms odd-order coherence intensity is shown separately for comparison and is indicative of the noise level. The largest change occurs between $r=0.25$ and 0.50. r is the fraction of methane in the reactant gases $[CH_4]/[(CH_4+SiH_4)]$.

trum because it only shows carbon nuclei which are not directly bound to hydrogen. As explained earlier, the ^{13}C-^{1}H dipolar coupling broadens the signal from hydrogenated carbon nuclei to the extent that it is indistinguishable from the base line. The peak at 120 ppm (sp^2) is essentially unchanged, indicating that there is virtually no hydrogen bound to the sp^2 carbons in this sample. The peak observed at 0 ppm (sp^3) in the left spectrum, has disappeared, showing that virtually all sp^3 carbons in this sample are hydrogenated.

Spectra with and without proton decoupling for samples $r=0.795$ and 0.875 are also shown in Fig. 5. These samples also show a significant amount of nonhydrogenated sp^2 bonding. The peaks near 120 ppm do not change with proton decoupling. In samples $r=0.795$ and 0.875, there is a small sp^3 peak in the spectra without decoupling which we assign to C—Si bonding. The presence of a small peak near 50 ppm most obvious in the $r=0.875$ sample (Fig. 5, bottom, right) is assigned to quaternary ("diamondlike") carbon environments.[20] As shown in Table I, the highest ratio of sp^2 to sp^3 carbon is found in the sample prepared from $r=0.25$. The percentage of sp^2 carbon decreases in the $r=0.795$ sample, but is a maximum in the $r=0.875$ sample. None of the samples contain any hydrogenated sp^2 carbon. The largest percentage of sp^3 carbon is found in the $r=0.795$ sample.

To determine if the sp^2 carbon is double bonded to other carbon atoms or to silicon, we observed the ^{29}Si NMR signal from these samples. No absorptions with chemical shifts greater than 100 ppm (relative to TMS), corresponding to Si=C,[22] were observed in these samples. Thus, the sp^2 carbons in these samples are in C=C configurations.

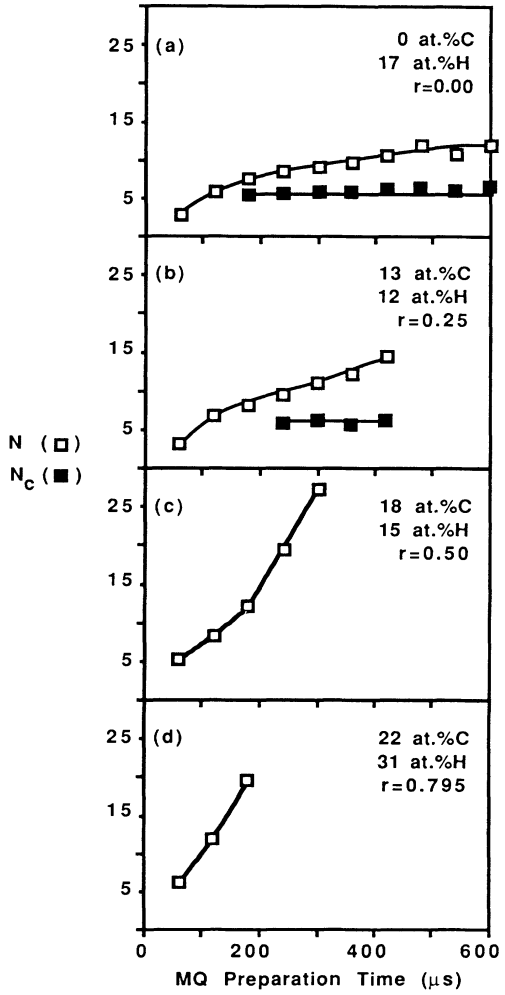

FIG. 4. The number of interacting hydrogen atoms N (open squares) and the number of hydrogen atoms in a cluster N_c (solid squares) as a function of MQ preparation time for four a-SiC:H samples. The uncertainty in both N and N_c is ± 1 hydrogen atom.

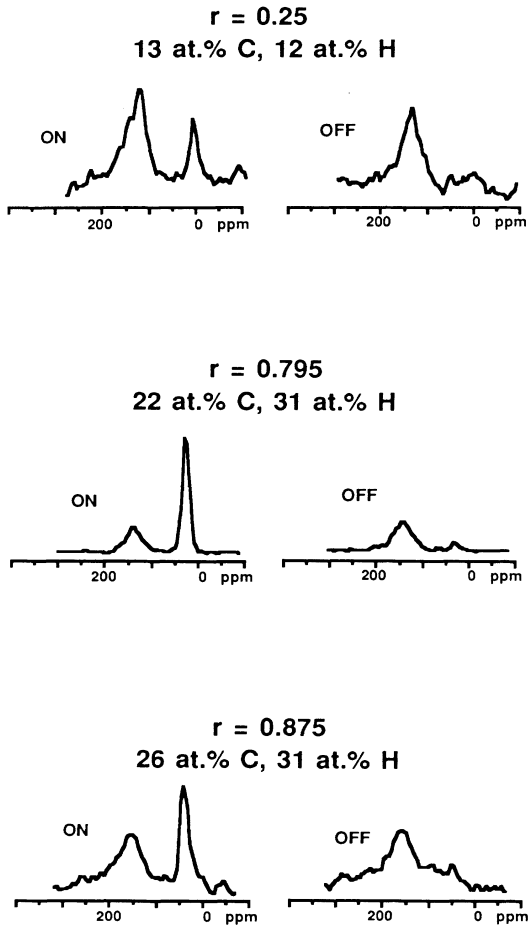

FIG. 5. ^{13}C-NMR spectra of a-SiC:H samples, plotted relative to tetramethylsilane. "ON" and "OFF" indicate spectra taken with and without proton decoupling, respectively. r is the fraction of methane in the reactant gases, $[CH_4]/[CH_4+SiH_4]$. These spectra were acquired with a magic-angle spinning rate of 4000 Hz.

TABLE I. Integrations of sp^2 (120 ppm) and sp^3 (0 ppm) peaks in spectra shown in Fig. 5. Also included are data for a sample prepared with $r=0.50$. The uncertainty in these values is ±0.5 at. %. r is the fraction of methane in the reactant gases, $[CH_4]/[(CH_4+SiH_4)]$.

Sample	Total sp^2 carbon (at. %)	Hydrogenated sp^2 carbon (at. %)	Total sp^3 carbon (at. %)	Hydrogenated sp^3 carbon (at. %)
$r=0.25$	9.9	<0.5	3.1	3.1
$r=0.50$	9.0	<0.5	9.0	9.0
$r=0.795$	6.3	<0.5	14.7	13.2
$r=0.875$	11.7	<0.5	11.3	10.1

The ir spectra show several changes with varying methane fraction in the reactant gas mixture. The various modes have been assigned previously.[23] With increasing carbon incorporation, the 770-cm^{-1} absorption (Si-C stretching mode) grows relative to the 640-cm^{-1} absorption (Si-H_n bending mode). The 880- and 800-cm^{-1} absorptions (Si-H_2 and $[Si\text{-}H_2]_n$ wagging modes, respectively) are only resolved in the first three samples of the series ($r \leq 0.50$). As the carbon content increases further, the 880- and 800-cm^{-1} absorptions either disappear or are small relative to the growing 770-cm^{-1} absorption. Absorptions near 3000 cm^{-1} (C-H_n stretching modes) are detected only in the higher-carbon-content samples ($r \geq 0.795$).

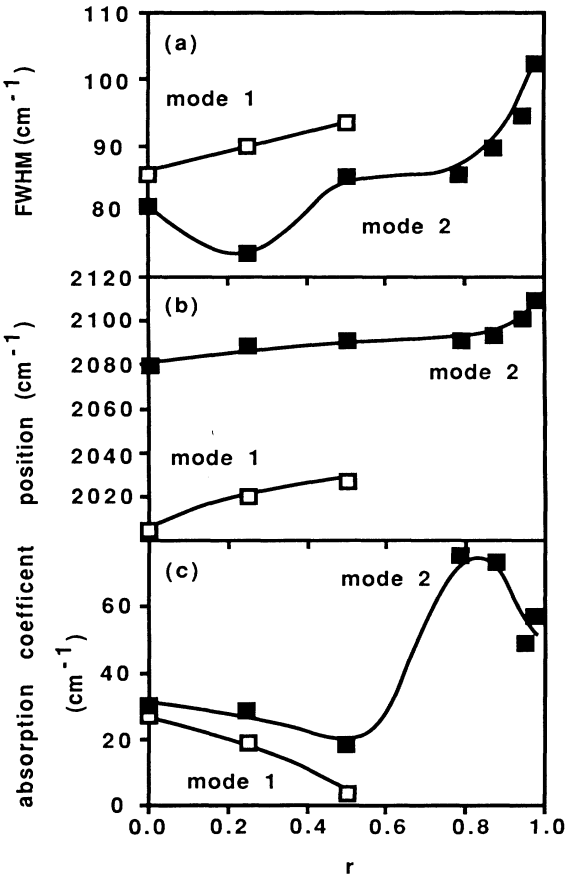

FIG. 6. The ir parameters for the two modes in the 2000–2200-cm^{-1} region vs r; full widths at half maximum (FWHM) (a), positions (b), and absorption coefficients. Mode 1 disappears at $r > 0.50$. The experimental uncertainties in these measurements are ±8 cm^{-1} in (a), ±4 cm^{-1} in (b), and ±10% in (c).

The ir spectrum of a-Si:H has two overlapping Gaussian absorption curves in the 2000–2200-cm^{-1} region (Si-H_n stretching modes). The first absorption is centered at 2000 cm^{-1} and the second absorption is centered at 2080 cm^{-1}. Both modes are also present in the first two a-SiC:H samples ($r=0.25$, 0.50). The linewidth [Fig. 6(a)] and position [Fig. 6(b)] of the first mode increase relative to a-Si:H, while the intensity [Fig. 6(c)] decreases. The remaining a-SiC:H samples ($r \geq 0.795$) have only one absorption in the 2000–2200-cm^{-1} region, corresponding to the second absorption of the lower-carbon-content samples. The linewidth of the second absorption [Fig. 6(a)] is smallest for the first a-SiC:H sample ($r=0.25$) and rapidly increases after the disappearance of the first mode ($r \geq 0.795$). The position of the second absorption [Fig. 6(b)] shifts to higher wave numbers as carbon content increases, with the greatest change occurring as the CH_4-(CH_4+SiH_4) ratio approaches unity. The intensity of the second absorption [Fig. 6(c)] decreases slightly for the $r=0.25$ and

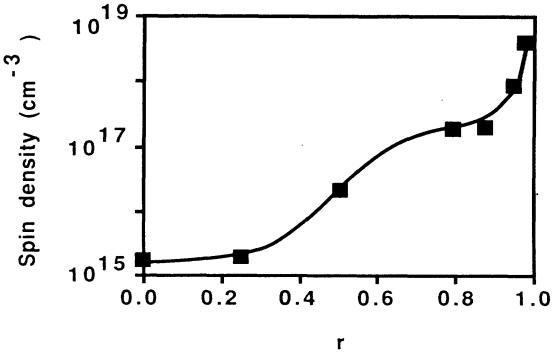

FIG. 7. The ESR spin density vs r. Note the variation over 4 orders of magnitude with carbon incorporation. The experimental error is $\pm 10^{14}$ spins/cm^3.

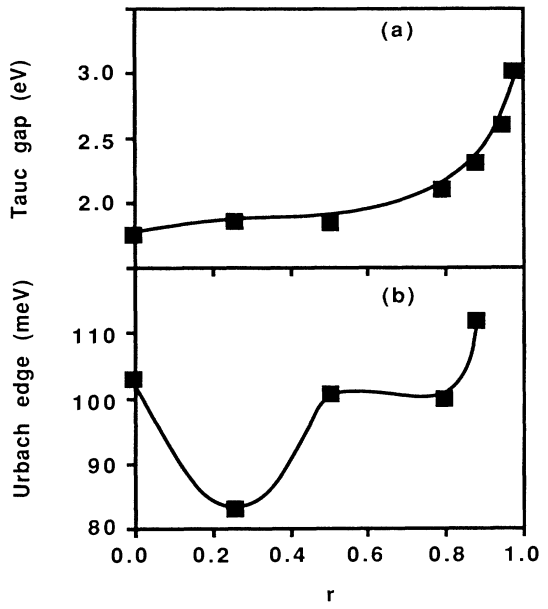

FIG. 8. Optical-absorption parameters vs r; (a) Tauc gap and (b) Urbach edge. The experimental error for these measurements is ± 0.1 eV for (a) and ± 5 meV for (b).

0.50 samples as compared to the a-Si:H sample. The next sample ($r=0.795$) shows a large increase in the intensity of the second mode, followed by a decrease as r increases further. This behavior is similar to that of the spin-lattice relaxation time constant [Fig. 2(a)].

The ESR measurements indicate that the spin density varies over four decades with carbon content (Fig. 7), in agreement with previous measurements.[4] The first a-SiC:H sample ($r=0.25$) has approximately the same spin density as the a-Si:H sample ($r=0.00$), while the remaining samples show a steady increase in spin density with carbon content. The g value decreased from the amorphous silicon value of 2.0055 with the addition of carbon. The linewidth (ΔH_{pp}) of the resonance varied between 6.5 to 8.5 G over the compositional range.

The changes in the optical-absorption data with increasing r are shown in Fig. 8. The Tauc gap [Fig. 8(a)] of the first two a-SiC:H samples ($r=0.25$, 0.50) is similar to the gap of the a-Si:H sample ($r=0.00$). The higher-carbon-content members of the series ($r \geq 0.795$) show a steady increase in the Tauc gap with increasing r. This dependence of the optical band gap on carbon content has been reported previously,[24,25] although cases of a smoother increase of the optical band gap with carbon content have also been observed.[5] Differences in deposition conditions may account for the two types of behavior. The Urbach edge [Fig. 8(b)] sharpens with the initial addition of carbon ($r=0.25$) and then broadens as the carbon content is increased further.

IV. DISCUSSION

A. Growth chemistry

For a random alloy, a continuous variation in material properties is expected with changing stoichiometry. However, within this compositional series of a-SiC:H films, two regions of variation are seen. Low-carbon-content films, produced from a gas mixture with a CH_4-(CH_4+SiH_4) ratio of less than 0.5, have growth rates [Fig. 1(a)], NMR linewidths [Fig. 2(c)], and optical band gaps [Fig. 8(b)], that are relatively insensitive to carbon content. In the low-carbon region, the hydrogen content [Fig. 1(b)], spin-lattice relaxation times [Fig. 2(a)], and ir absorption coefficients [Fig. 6(c)] are slightly lower than those of a-Si:H. In the higher-carbon-content films these properties are very different. The origin of these two regions will be discussed further in terms of differences in deposition chemistry and film microstructure.

The deposition rates of low-carbon-content a-SiC:H ($r<0.50$) and a-Si:H are similar, but the deposition rate of the high-carbon-content films decreases dramatically [Fig. 1(a)]. This decrease could result from a number of mechanisms: lower concentrations of plasma species capable of participating in heterogeneous reactions, a change in surface chemistry which reduces the number or activity of film-growth sites, or an increase in plasma species capable of removing atoms from the growing film. The carbon-to-silicon ratio in the film is much less than the CH_4-SiH_4 ratio in the plasma, indicating that CH_4 is less reactive than SiH_4, in agreement with the fact that C—H bonds are stronger than Si—H bonds. However, carbon incorporation does not vary linearly with the fraction of CH_4 in the gas phase [Fig. 1(b)], indicating that the formation of reactive carbon-containing intermediates is not the only important step in the growth mechanism. For example, the removal of hydrogen atoms from the growing surface with subsequent formation of a reactive dangling bond has been proposed as the rate-limiting step in an a-Si:H growth mechanism.[26] At a constant substrate temperature of 270 °C, low-carbon-content films ($r<0.50$) contain less than 20 at. % H, while the high-carbon-content films contain more than 30 at. % H [Fig. 1(a)]. This suggests that the rate of hydrogen elimination decreases nonlinearly with carbon incorporation. Our results also seem to indicate that there is a threshold amount of methane required before carbon affects the film properties.

The ^{13}C NMR results demonstrate that carbon-carbon bonding is present in all of these films, even at low carbon concentrations. Additionally, the majority of the sp^2 carbon-bonding environments are not hydrogenated. Thus, when attempting to explain the behavior of this alloy system, it is important to consider the heterogeneity of not only the hydrogen microstructure, but of the carbon-bonding environments as well. It is worth noting that the variation in carbon-bonding environments may be rationalized in terms of CH_4 gas-phase discharge chemistry. Mass spectrometric studies[27,28] show that higher hydrocarbons are formed in methane plasmas. We speculate that these intact higher hydrocarbons are incorporated into the growing film, leading directly to carbon-carbon bonding within the film. Larger hydrocarbon species should adsorb on the growing surface more readily than smaller hydrocarbon species, making the incorporation of carbon-carbon bonds very likely.

Evidence for an adsorption-dependent growth rate has been seen in studies of amorphous carbon deposition. As the substrate temperature decreased, the growth rate of amorphous carbon increased, implying that more reactive species remained on the growing surface at lower substrate temperatures.[29]

Proton NMR measurements demonstrate that the hydrogen microstructure differs significantly between the two types of films. First, the Lorentzian fraction of the single-quantum NMR spectra [Fig. 2(b)], indicative of isolated hydrogen environments, decreases with increasing r, indicating that more hydrogen is incorporated into clustered environments (Gaussian line shape) with increasing carbon content. The linewidth of the NMR absorption due to clustered environments in the low-carbon-content films [Fig. 2(c)] remains similar to the a-Si:H value. However, the width of the Gaussian line shape increases for the high-carbon-content films, corresponding to smaller average separation of hydrogen atoms perhaps because of the inclusion of $—CH_2$, $—CH_3$, or $(—CH_2)_n$ species, which have smaller H-H separations than their silicon analogs and were observed in the ir and ^{13}C NMR spectra of these samples. The spin-lattice relaxation (T_1) behavior [Fig. 2(a)] confirms a change in film morphology between the low- and high-carbon-content films. However, the details of the behavior are difficult to explain since it depends on both the number of T_1 relaxation centers in the films, such as trapped H_2, $—CH_3$, or $—SiH_3$ groups, and their geometric relationship to the remaining bound hydrogen atoms.[8]

B. Film microstructure

Multiple-quantum NMR provides insight about the microstructure of the hydrogenated regions. Consider first the a-Si:H film and the a-SiC:H film with the least amount of carbon ($r=0.25$). The most likely explanation of the MQ NMR data for these films [Figs. 4(a) and 4(b)] is that the constant value of N_c indicates that hydrogen exists in clusters of 5–7 atoms and the gradual increase in N with increasing preparation time indicates that these clusters are not completely isolated from each other. The greater increase of N with increasing preparation time in the a-SiC:H film indicates that the clusters are closer together in the carbon containing material. The observations of lower hydrogen content and smaller intercluster distance in the a-SiC:H film support the ^{13}C NMR conclusion that areas of the a-SiC:H films are devoid of hydrogen. The ^{13}C NMR of this sample indicates the majority of carbon is bonded in the sp^2 configuration and is not bonded to hydrogen. The similarities between the a-Si:H film and the low-carbon-content a-SiC:H film suggest that the a-SiC:H film has a heterogeneous structure consisting of nonhydrogenated carbon inclusions in an "amorphous-silicon-like" lattice. Most likely, the hydrogen concentration of this film is lower than that of a-Si:H simply because the volume fraction of the amorphous-silicon-like lattice is reduced by the incorporation of the nonhydrogenated sp^2 carbon regions. Based on lattice geometry considerations, previous authors[30] have suggested that carbon clusters will replace silicon-silicon bonds, since the C-C-C nearest-neighbor distance is 4.12 Å in diamond and 4.26 Å in graphite, matching the Si—Si bond length of 3.8 Å in crystalline silicon more closely than a C—C bond length of 2.52 Å in diamond or 2.46 Å in graphite.

The MQ NMR results of films produced from $r=0.5$ and 0.795 are shown in Figs. 4(c) and 4(d). Groups of more than 25 interacting hydrogen atoms are observed. The existence of large hydrogen clusters in the sample of Fig. 4(c) ($r=0.50$) is unexpected, since this sample contains only 15 at. % H, less than the 17 at. % H in the a-Si:H film. This indicates that regions of the film devoid of hydrogen are interspersed between large hydrogen clusters. However, the ^{13}C NMR spectra of this material show that the fraction of hydrogenated sp^3 carbon has increased over that of the $r=0.25$ film. Apparently, the addition of nonhydrogenated sp^2 carbon regions to an amorphous silicon lattice has little effect on the hydrogen microstructure of the resulting material. However, the addition of sp^3 hydrogenated carbon has a profound effect on both the hydrogen microstructure and the film properties. For the highest-carbon-content sample in Fig. 4(d) ($r=0.795$), these large hydrogen clusters are a plausible structure because the film contains 31 at. % H. Interestingly, this film is the first in the compositional series to have optical properties that differ significantly from those of a-Si:H. These MQ NMR results indicate that the hydrogen microstructure is no longer amorphous-silicon-like with small hydrogen clusters, but contains large numbers of hydrogen atoms close to one another. The ^{13}C NMR shows that this film has more sp^3 carbon than sp^2, and that this sp^3 carbon is hydrogenated. This is supported by the appearance of $C—H_n$ bond-stretching modes near 3000 cm^{-1} in the ir absorption spectra.

It seems that the difference between the amorphous-silicon-like films and the higher-carbon-content films is caused by the increase in hydrogen content and the increase in sp^3 carbon contents. Unfortunately, within this series of films, these two effects are indistinguishable. In our films, increasing the carbon content increases both the sp^3 carbon content and the hydrogen content. It would be interesting to prepare a series of films where these properties were not coupled.

The ir spectra also support the hypothesis that there are low-carbon-content amorphous-silicon-like materials and higher-carbon-content amorphous-silicon-carbide-like materials in this compositional series. The absorption peak near 2000 cm^{-1} (stretching mode of isolated Si-H) appears in only the low-carbon-content films [Fig. 6(c)], while the absorption peaks near 3000 cm^{-1} ($C-H_n$ stretching modes) appear only in the high-carbon-content films. Prior to its disappearance, the position of the 2000-cm^{-1} absorption shifts to a higher wave number with increasing carbon content [Fig. 6(b)], probably due to back bonding of the silicon atoms to carbon.[23] The 2080-cm^{-1} absorption (stretching mode of clustered Si-H) also shifts to higher wave number, but the increase may, in part, be due to a change in the local dielectric constant owing to a transition from small well-ordered

clusters to large ill-defined groups of hydrogen atoms.[31] The increase in absorption coefficient of the 2080-cm^{-1} absorption between the low- and high-carbon-content films [Fig. 6(c)] reflects their difference in hydrogen content. The subsequent decrease in the 2080-cm^{-1} mode in the high-carbon region could be indicative of increasing C-H_n to Si-H_n ratios with increasing carbon incorporation. This hypothesis is supported by the appearance of the 3000-cm^{-1} absorptions. It is interesting to note the similar behavior of the absorption coefficient of the 2080-cm^{-1} mode [Fig. 6(c)] and the NMR spin-lattice relaxation time constant [Fig. 2(a)] with increasing r.

C. Optical properties

The nonlinear behavior of the optical band gap with carbon incorporation [Fig. 8(a)] also supports the hypothesis of two microstructural regimes within the series. The low-carbon-content films are particularly puzzling. The addition of 18 at. % C does *not* increase the optical band gap significantly as compared to amorphous silicon. This is contrary to the increase in the gap predicted by a simple tight-binding calculation for tetrahedral solids.[32] However, these are not tetrahedral solids; 9 at. % C is incorporated in the sp^2 configuration. One could rationalize the failure of sp^2 carbons to increase the gap of amorphous silicon on the basis of observations that the π-to-π^* transition of this configuration is smaller in energy than the σ-to-σ^* transition in the tetrahedral environment.[33] However, 9 at. % C is incorporated in the sp^3 configuration without increasing the optical gap significantly. An electronic model which accounts for the heterogeneous nature of the structure and composition may be required. One possibility is the quantum-well model for amorphous silicon[34] could be extended for a-SiC:H such that the optical gap would be controlled by the amorphous-silicon-like regions in the low-carbon-content films. Perhaps the slight increase in the Tauc gap in these films is related to the increasing hydrogen content of the amorphous-silicon-like regions of the films, even though the total hydrogen content remains constant. Finally, in higher-carbon-content samples, the optical band gap increases considerably with the addition of carbon atoms. This behavior is consistent with tight-binding calculations based upon the increased s-p splitting of atomic carbon *vis-a-vis* silicon. This is not to be taken as an endorsement of the tight-binding approach for these alloys. Indeed, the gross heterogeneity of these high-carbon-content films suggests their treatment more as polymers than as semiconductors.

In other studies of a-SiC:H compositional series, similar behavior of the optical band gap with carbon incorporation has been observed.[25] In those studies, a sharp decrease in the ratio of the photoconductivity to the dark conductivity begins when the optical band gap begins to increase. Other authors have suggested that microvoid structure is an important cause of the degradation in photoresponse of a-SiC:H and that the 2080-cm^{-1} ir absorption is correlated with this microstructure.[35] We suggest that the 2080-cm^{-1} absorption is caused by the clustered hydrogen in a-SiC:H, as in amorphous silicon,[14] and the shift to higher wave numbers and increase in width of this absorption in the high-carbon-content samples is indicative of the loss of an ordered hydrogen microstructure, as measured by MQ NMR.

The ESR spin density is small ($<10^{16}$ cm^{-3}) for the low-carbon-content samples with amorphous-silicon-like lattice structure (Fig. 7). The loss of this structure in higher-carbon-content films correlates with a dramatic rise in the spin density. Increased unpaired spin density in a-SiC:H contributes to, but is not entirely responsible for, decreased photoconductivity.[4]

The width of the Urbach edge is a measure of disorder in amorphous materials, with broader edges signifying a greater distribution of states in the valence-band tail.[36] Another measure of disorder is the width of the ir absorption peaks.[37] Both the Urbach edge [Fig. 8(b)] and the 2080-cm^{-1} absorption mode in the ir spectra [Fig. 6(a)] narrow with the initial addition of carbon, suggesting a more ordered film. Photosensitivity measurements[25] have also shown a decrease in the density of valence-band-tail states with the addition of up to 20 at. % carbon. We suggest that for $r \leq 0.5$, the films are less disordered because the nonhydrogenated sp^2 carbon regions act as strain relievers in the lattice. Films in the higher-carbon-content regime have wider Urbach edges and wider 2080-cm^{-1} ir absorptions, indicating more disorder in these films, also in agreement with the photosensitivity measurements.[25] The increase in disorder for $r > 0.5$ is probably caused both by the inability of the hydrogen atoms to exist in well-ordered clusters as well as compositional disorder resulting from the plethora of silicon, carbon, and hydrogen local-bonding environments.

V. CONCLUSIONS

The most important conclusion is that amorphous hydrogenated silicon carbide is heterogeneous. All films in this study contain both sp^3 (tetrahedral) and sp^2 (planar) carbon-bonding environments. The sp^3 carbon is predominantly hydrogenated while the sp^2 carbon have no bound hydrogen. Two types of microstructure are present in the compositional series. At low carbon contents (<20 at. %), this alloy system forms amorphous-silicon-like lattices, containing clusters of 6 ± 1 hydrogen atoms and regions devoid of hydrogen, due to inclusions of nonhydrogenated sp^2 carbon. Higher-carbon-content samples also consisted of hydrogenated and nonhydrogenated regions, but did not have the well-defined hydrogen microstructure of the lower-carbon-content films. Also, there is a greater fraction of sp^3 carbon in the higher-carbon-content films.

Neither type of hydrogen microstructure is indicative of a low-defect, random tetrahedral alloy. Low-carbon-content films had few unpaired electrons and a low amount of disorder; however, the optical band gaps are insensitive to carbon incorporation. At high carbon content, optical band gaps could be tailored by carbon

incorporation; however, these materials contain large unpaired electron densities and increased amounts of disorder and microstructure. The importance of growth chemistry in determining microstructure is reflected in the different growth rates of the two regimes. Novel deposition methods which improve the hydrogen-elimination reactions and/or carbon-atom incorporation may be necessary to achieve a low-defect, random tetrahedral alloy. Both the direct structural changes associated with the incorporation of carbon atoms and the concomitant changes in the hydrogen microstructure, affect the optoelectronic properties of *a*-SiC:H films. The consequences of these results on device physics and theory have yet to be determined.

ACKNOWLEDGMENTS

We thank Constance Gettinger for measuring the optical band gaps and Paul Skerker for assistance with the ESR measurements. This work was supported by the National Science Foundation through Grant No. DMR-83-04163.

*Current address: Department of Chemical Engineering, Northwestern University, Evanston, IL 60201.

†Current address: Department of Chemical Engineering, MIT, Cambridge, MA 02139.

[1]D. E. Carlson, J. Vac. Sci. Technol. **20**, 290 (1982).

[2]Y. Tawada, K. Tsuge, M. Kondo, H. Okamoto, and Y. Hamakawa, J. Appl. Phys. **53**, 5273 (1982).

[3]D. A. Anderson and W. E. Spear, Philos. Mag. B **35**, 1 (1977).

[4]A. Morimoto, T. Miura, M. Kumeda, and T. Shimizu, J. Appl. Phys. **53**, 7299 (1982).

[5]J. Bullot, M. Gauthier, and M. Schmidt, Philos. Mag. B **49**, 489 (1984).

[6]A. H. Mahan, B. von Roedern, D. L. Williamson, and A. Madan, J. Appl. Phys. **57**, 2717 (1985).

[7]J. Tafto and F. J. Kampas, Appl. Phys. Lett. **46**, 949 (1985).

[8]P. C. Taylor, in *Semiconductors and Semimetals,* edited by Jacques I. Pankove (Academic, Orlando, 1984), Vol. 21C, pp. 99–154.

[9]S. Kaplan and A. Dilks, Thin Solid Films **84**, 419 (1981).

[10]J. Baum, K. K. Gleason, A. Pines, A. N. Garroway, and J. A. Reimer, Phys. Rev. Lett. **56**, 1377 (1986).

[11]J. A. Reimer, R. W. Vaughan, J. C. Knights, and R. A. Lujan, J. Vac. Sci. Technol. **19**, 53 (1981).

[12]T. C. Farrar and E. D. Becker, *Pulse and Fourier Transform NMR* (Academic, New York, 1971).

[13]Y. S. Yen and A. Pines, J. Chem. Phys. **78**, 3579 (1983); J. Baum, M. Munowitz, A. N. Garroway, and A. Pines, *ibid.* **83**, 2015 (1985); J. Baum and A. Pines, J. Am. Chem. Soc. **104**, 7447 (1986).

[14]K. K. Gleason, M. A. Petrich, and J. A. Reimer, Phys. Rev. B **36**, 3259 (1987).

[15]B. C. Gerstein and C. R. Dybowski, *Transient Techniques in NMR of Solids* (Academic, New York, 1985), pp. 234–239.

[16]E. R. Andrew, in *Progress in NMR Spectroscopy,* edited by J. W. Emsley (Pergamon, New York, 1972), Vol. 8, pp. 1–40.

[17]J. Tauc, *Amorphous and Liquid Semiconductors* (Plenum, New York, 1974), Chap. 4.

[18]F. Urbach, Phys. Rev. **92**, 1324 (1953).

[19]K. Nakazawa, S. Ueda, M. Kumeda, A. Morimoto, and T. Shimizu, Jpn. J. Appl. Phys. **21**, L176 (1982).

[20]T. M. Duncan, J. Phys. Chem. Ref. Data **16**, 125 (1987).

[21]Gordon R. Finlay, J. Stephen Hartman, Mary F. Richardson, and Barbara L. Williams, J. Chem. Soc. Chem. Commun. **1985**, 159 (1985).

[22]A. G. Brook, K. D. Safa, P. Lickiss, and K. M. Baines, J. Am. Chem. Soc. **107**, 4338 (1985).

[23]H. Wieder, M. Cardona, and C. R. Guarnieri, Phys. Status Solidi B **92**, 99 (1979).

[24]P. Chaudhuri, S. Ray, A. K. Batabyal, and A. K. Barua, Thin Solid Films **121**, 233 (1984).

[25]N. Saito, N. Tanaka, and I. Nakaaki, Appl. Phys. A **38**, 37 (1985).

[26]B. A. Scott, J. A. Reimer, and P. A. Longeway, J. Appl. Phys. **14**, 6853 (1983).

[27]W. D. Partlow and L. E. Kline, Mater. Res. Soc. Symp. Proc. **68**, 309 (1986).

[28]J. Wagner, Ch. Wild, A. Bubenzer, and P. Koidl, Mater. Res. Soc. Symp. Proc. **68**, 205 (1986).

[29]M. A. Petrich and J. A. Reimer (unpublished).

[30]Y. Katayama, K. Usami, and T. Shimadi, Philos. Mag. B **43**, 283 (1981).

[31]H. Wagner and W. Beyer, Solid State Commun. **48**, 585 (1983).

[32]W. A. Harrison, *Electronic Structure and the Properties of Solids* (Freeman, San Francisco, 1980).

[33]L. Lang, *Absorption Spectra in the Ultraviolet and Visible Region* (Academic, New York, 1961), Vol. 1, p. 31ff.

[34]M. H. Brodsky, Solid State Commun. **36**, 55 (1980).

[35]A. H. Mahan, P. Raboisson, and R. Tsu, Appl. Phys. Lett. **50**, 335 (1987).

[36]J. Singh, Phys. Rev. B **23**, 4256 (1981).

[37]D. E. Soule, G. T. Reedy, E. M. Peterson, and J. A. McMillan, in *Tetrahedrally Bonded Amorphous Semiconductors (Carefree, Arizona),* Proceedings of a Topical Conference on Tetrahedrally Bonded Amorphous Semiconductors, AIP Conf. Proc. No. 73, edited by R. A. Street, D. K. Biegelsen, and J. C. Knights (AIP, New York, 1981), p. 89.